Title	CABYR is essential for fibrous sheath integrity and progressive motility in mouse spermatozoa
Author(s)	Young, Samantha A.M.; Miyata, Haruhiko; Satouh, Yuhkoh et al.
Citation	Journal of Cell Science. 2016, 129(23), p. 4379-4387
Version Type	VoR
URL	https://hdl.handle.net/11094/78592
rights	
Note	

The Company of Biologists

RESEARCH ARTICLE

CABYR is essential for fibrous sheath integrity and progressive motility in mouse spermatozoa

Samantha A. M. Young[1,2], Haruhiko Miyata[2], Yuhkoh Satouh[3], Robert John Aitken[1], Mark A. Baker[1] and Masahito Ikawa[2,3,*]

ABSTRACT

Ca^{2+}-binding tyrosine-phosphorylation-regulated protein (CABYR) has been implicated in sperm physiological function in several *in vitro* studies. It has also been implicated as a potential cause of and diagnostic tool in asthenozoospermic human males. CABYR is known to be localized to the fibrous sheath, an accessory structure in the flagellar principal piece. Utilizing the CRISPR–Cas9 technology, we have knocked out this gene in mice to understand its role in male fertility. *Cabyr*-knockout male mice showed severe subfertility with a defect in sperm motility as well as a significant disorganization in the fibrous sheath. Further, abnormal configuration of doublet microtubules was observed in the *Cabyr*-knockout spermatozoa, suggesting that the fibrous sheath is important for the correct organization of the axoneme. Our results show that it is the role of CABYR in the formation of the fibrous sheath that is essential for male fertility.

KEY WORDS: Spermatozoa, Knockout, CRISPR–Cas9, CABYR, Fibrous sheath

INTRODUCTION

Spermatozoa are unique and highly specialized cells. They comprise a head region, where the paternal genetic information is stored, and the flagellum, which propels the cell towards its ultimate destination, the oocyte. The flagellum is made up of four segments: the connecting piece directly adjacent to the head; the midpiece containing the mitochondrial gyres wrapped around the axoneme; the principal piece, which is enclosed by the fibrous sheath; and a short end piece (Eddy et al., 2003; Li et al., 2011). The principal piece makes up about three quarters of the flagellum and is largely responsible for forming the flagellar beat, the wave-like pattern that propels spermatozoa towards to the oocyte (Eddy et al., 2003; Li et al., 2011). Within the principal piece exists a unique cytoskeletal structure known as the fibrous sheath. The fibrous sheath surrounds the axoneme and outer dense fibres, and contains two longitudinal columns that are connected by closely organized semicircular transverse ribs. The fibrous sheath is believed to regulate the degree of flexibility, flagellar motion and shape of the flagellar beat during the lifespan of a sperm cell (Eddy et al., 2003). The main structural components of the fibrous sheath come from two proteins of the

A-kinase anchoring family (AKAPs), which includes AKAP3 and AKAP4 (Fiedler et al., 2013). As such, the fibrous sheath acts as a scaffold for several signalling and/or metabolic pathways (Li et al., 2010). For example, many glycolytic enzymes are found along the fibrous sheath that enable local energy production for sperm motility (Li et al., 2011; Nakamura et al., 2013; Bunch et al., 1998; Krisfalusi et al., 2006; Westhoff and Kamp, 1997; Feiden et al., 2007).

In addition to glycolytic enzymes, another protein bound to the fibrous sheath is the Ca^{2+}-binding tyrosine-phosphorylation-regulated (CABYR) protein (Naaby-Hansen et al., 2002). The importance of this protein first came to light when studies demonstrated that CABYR becomes phosphorylated during sperm capacitation (Naaby-Hansen et al., 2002). Capacitation is the biochemical process sperm undergo after ejaculation, within the female reproductive tract and is necessary for fertilization to take place (Yanagimachi, 1994). This first report was followed by papers that defined the specific phosphorylated peptides of CABYR that are involved in tyrosine phosphorylation during sperm capacitation (Ficarro et al., 2003), and by mapping of the Ca^{2+}-binding domain to a particular region of CABYR (Kim et al., 2005). Ca^{2+} is known to play an essential role in both capacitation and sperm motility (Navarrete et al., 2015; Ho and Suarez, 2003).

Although a role for CABYR during capacitation is plausible, the expression profile of CABYR strongly suggests that this protein is likely to play another role in the development of the fibrous sheath. During spermiogenesis, whereupon a round cell is converted into a sperm cell, up to 16 different steps have been classified (Meistrich et al., 2003). During stages 14–16, the development of the fibrous sheath occurs. It is at step 14 that CABYR is first detected in the developing flagella (Li et al., 2010). Furthermore, CABYR is still present in step-16 spermatids when the fibrous sheath is complete (Li et al., 2010; Sakai et al., 1986). This suggests that CABYR is strongly linked to the development of the fibrous sheath during spermatogenesis. Indeed, the N-terminal domain of CABYR (residues 12–48) has high homology to the RIIα domain of protein kinase A (PKA) (Sen et al., 2003). This region is known as the R2D2 domain (Colledge and Scott, 1999; Sen et al., 2003), and several other proteins also have this motif (Hanlon Newell et al., 2008; Kim et al., 2005; Li et al., 2010). Through this R2D2 domain, CABYR has been shown to bind to the main protein structural components of the fibrous sheath, AKAP3 and AKAP4.

Nevertheless, despite the binding evidence and data on staging and temporal expression during spermiogenesis that suggest CABYR could be involved in the development of the fibrous sheath, to date, no definitive evidence has been found to confirm this. As such, this study utilized the genetic technology of the CRISPR–Cas9 system to generate a *Cabyr*-knockout (KO) mouse line. Spermatozoa derived from this line demonstrate the

[1]Priority Research Centre in Reproductive Science, Discipline of Biological Sciences, Faculty of Science and IT, University of Newcastle, Callaghan, New South Wales 2308, Australia. [2]Department of Experimental Genome Research, Research Institute for Microbial Diseases, Osaka University, Suita, Osaka 565-0871, Japan. [3]Animal Resource Center for Infectious Diseases, Research Institute for Microbial Diseases, Osaka University, Suita, Osaka 565-0871, Japan.

*Author for correspondence (ikawa@biken.osaka-u.ac.jp)

M.I., 0000-0001-9859-6217

Journal of Cell Science

importance of CABYR in the correct formation and structure of the fibrous sheath.

RESULTS

Generation of *Cabyr*-KO mice

We found seven *Cabyr* splice variants by using an *in silico* search (www.ensembl.org) (Fig. 1A). The single guide RNA (sgRNA) target was designed in exon 2 because that exon contains the initial methionine and is shared by all of the transcripts (Fig. 1A,B). *Cabyr*-KO mice were generated by microinjecting oocytes with 5 ng/μl of pX330 plasmid that expressed both sgRNA and Cas9 protein (Mashiko et al., 2013). Of the 149 fertilized oocytes that had been injected, 117 were transplanted into the oviducts of pseudopregnant females and nine pups were born. Of these nine pups, one male mouse possessed a mutation that was mosaic. Insertion of the mosaic pup genome into a pBluescript cloning vector allowed us to determine the changes to the alleles – a 17-bp insertion, a 135-bp deletion and a 1-bp insertion. This mosaic mouse was caged with two wild-type (WT) females for approximately three months to expand the colony, but no pups were born. Superovulated females were then mated with this male mouse and the spermatozoa were flushed from the uterus. The morphology and motility of the spermatozoa appeared to be normal when viewed by performing conventional microscopy. One epididymis was then collected for *in vitro* fertilization (IVF). However, no fertilized oocytes were obtained. Therefore, we decided to use the remaining epididymis to perform intracytoplasmic sperm injection (ICSI). Through ICSI, 11 pups were born, 6 out of 11 were WT, and 5 out of 11 were heterozygous (1 out of 5 had a 1-bp insertion, 2 out of 5 had a 135-bp

deletion and 2 out of 5 had a 17-bp insertion). The mice with the 17-bp insertion were bred to obtain homozygous mice (*Cabyr*$^{+17/+17}$ KO mice; Fig. 1C). The 17-bp insertion resulted in a premature stop codon in exon 3 (also transcribed in all splice variants) and the production of a CABYR protein that was only 60 amino acids in length. The obtained *Cabyr*$^{+17/+17}$ KO mice were viable and showed no overt abnormalities.

Confirmation of deletion of CABYR in the KO mouse line

In order to demonstrate that CABYR was absent in the *Cabyr*-KO spermatozoa, immunoblotting was performed (Fig. 2A). As shown, a strong band of approximately 86 kDa was present in the heterozygous sample but absent in the KO sample. Other bands, including 50-kDa and 30-kDa isoforms (Li et al., 2010), were not detectable in the *Cabyr*-KO sample. Immunocytochemical analysis confirmed previous reports (Naaby-Hansen et al., 2002) that CABYR is localized to the principal piece of the sperm tail obtained from heterozygous mice. Further, we could not see any signal in the spermatozoa obtained from the *Cabyr*-KO mice (Fig. 2B), indicating that CABYR is absent in the KO spermatozoa. It should be noted that sperm morphology appeared normal in the *Cabyr*-KO mice under conventional microscopy. Further analysis of the subcellular localization of CABYR with super-resolution imaging revealed multiple and separated lines of signals observed in the principal piece, which is consistent with the previous findings (Naaby-Hansen et al., 2002; Li et al., 2010) that showed the location of CABYR in the fibrous sheath (Fig. 2C). To determine if the loss of CABYR affected the two major structural components of the fibrous sheath, we performed immunoblots using antibodies against AKAP3 and AKAP4 (Li et al., 2011). In both cases, the amount of these proteins remained unchanged in the *Cabyr*-KO spermatozoa (Fig. 2D).

Male fertility analysis

Breeding of *Cabyr*-KO males with WT females for a period of 3 months demonstrated severe subfertility (Fig. 3A). From three months of mating, only a single pup was born that was sired by a *Cabyr*-KO male. This indicated that although the spermatozoa looked morphologically normal, there were still defects causing this fertility phenotype. *In vitro* analysis showed a significant loss in the ability of the KO spermatozoa to fertilize in IVF assays of oocytes both with an intact cumulus cell layer (cumulus-intact) and with the cumulus cell layer removed (cumulus-free) (Fig. 3B). Although several other gene-KO mouse lines have been generated whose spermatozoa cannot bind to the zona pellucida, an extracellular matrix surrounding the oocyte (Ikawa et al., 2010; Fujihara et al., 2014; Okabe, 2013), *Cabyr*-KO spermatozoa could still bind to the zona pellucida (Fig. 3C; Fig. S1A). Further, when the zona pellucida was removed, KO spermatozoa continued to fuse with the oocyte (Fig. 3D), suggesting that knockout of *Cabyr* does not affect sperm–egg interaction at the oolemma. Taken together with the results using cumulus- and zona-intact eggs, these findings indicate that knockout of *Cabyr* impairs the ability of spermatozoa to penetrate the zona pellucida but not sperm–egg binding and fusion. Consistent with this idea, *Cabyr*-KO spermatozoa can undergo the acrosome reaction (Fig. S1B,C) that is a prerequisite for sperm–oocyte membrane fusion (Inoue et al., 2011a).

Fig. 1. CABYR isoforms and CRISPR–Cas9 strategy. (A) Isoforms of CABYR in the mouse. Closed bars indicate translated exons, open bars indicate untranslated exons. Grey bars indicate isoforms degraded through nonsense-mediated decay (NMD). (B) Forward (Fw) and reverse (Rv) primers surrounding the sgRNA-target region (black arrows); PAM sequence shown in red. Blue arrowhead indicates site of Cas9 digestion, underlined region indicates sgRNA-target sequence. (C) Sequence analysis of WT (top row) versus KO (bottom row), 17-bp insertion indicated by open bracket.

Motility analysis

Motility is one of the most important aspects of the ability of a spermatozoan to fertilize an oocyte (Suarez et al., 1993; Miyata
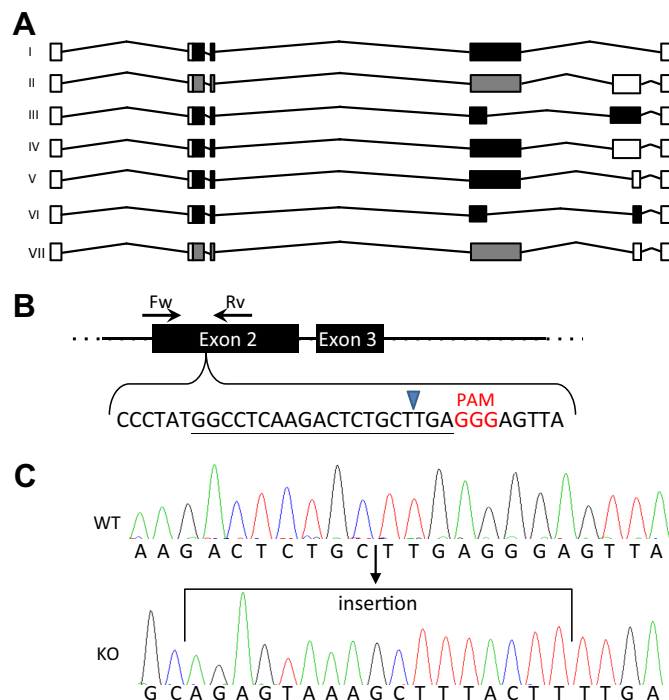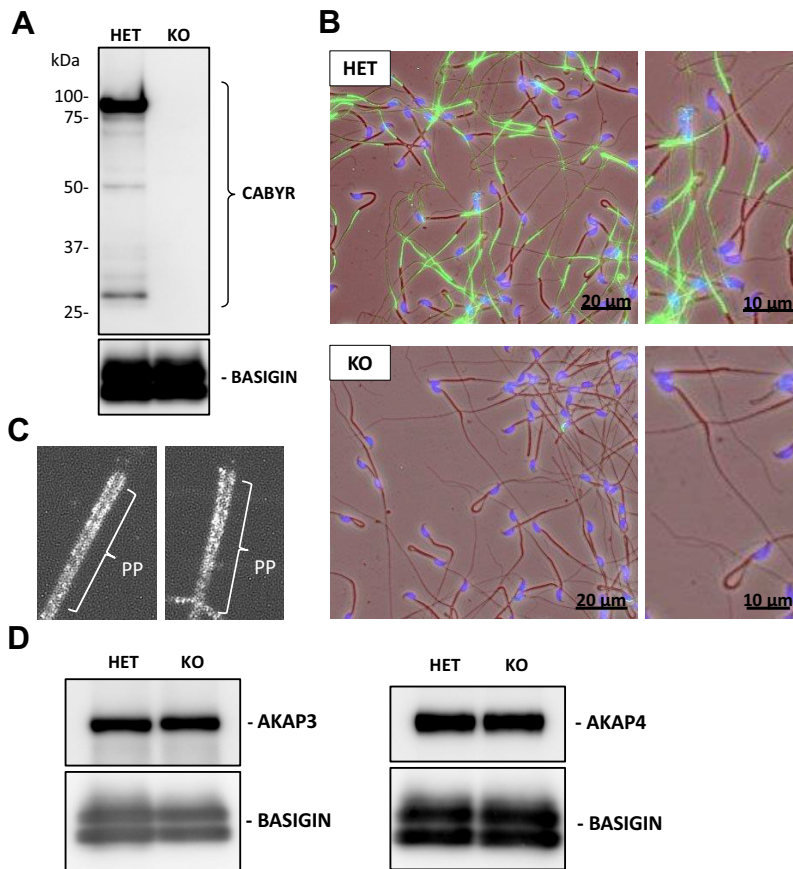
Fig. 2. Confirmation of knockout of *Cabyr*. (A) Immunoblot analysis of CABYR in *Cabyr* heterozygote (+/*Cabyr*$^{+17}$; HET) and homozygote (*Cabyr*$^{+17/+17}$; KO). (B) Immunostaining analysis of CABYR using spermatozoa from HET and KO mice. Green, CABYR; blue, nuclear staining. (C) Super-resolution images of CABYR expression in the principal piece (PP) of WT spermatozoa. Two examples are shown. (D) Immunoblot analysis of AKAP3 and AKAP4 expression in *Cabyr* HET and KO spermatozoa. Basigin as control.

et al., 2015). Owing to the location of CABYR (Fig. 2B), we hypothesized that the fertility defect is be due to impaired sperm motility. We analyzed sperm motility using computer-assisted spermatozoa analysis (CASA). In Toyoda, Yokoyama and Hoshi (TYH) medium (Toyoda et al., 1971), which induces capacitation, the *Cabyr*-KO spermatozoa had significantly lower total (percentage of motile cells) and progressive (percentage of cells moving forward) motilities (Fig. 4A,B). Similar defects were observed when the spermatozoa were incubated in non-capacitating medium (Fig. S2A), suggesting that capacitation signalling was not the cause of the defects. The KO spermatozoa also had significantly lower average path velocity (VAP), straight line velocity (VSL) and curvilinear velocity (VCL) at both 10 min and 120 min of incubation (Fig. 4C, Movies 1, 2). The occurrence of hyperactivation, a qualitative change in the mode of sperm motility during capacitation, was also significantly lower in the KO mice after 2 h (Fig. S2B), which could be caused by impaired basal motility because sperm motility is even lower in non-capacitating medium (Fig. S2A). These data indicated that motility defects were the most likely cause of the failure of spermatozoa to penetrate the zona pellucida.

Tyrosine and PKA phosphorylation

CABYR is phosphorylated on tyrosine as well as on serine and threonine residues during capacitation, which is thought to be involved in the capacitation process (Ficarro et al., 2003; Kim et al., 2005; Naaby-Hansen et al., 2002). To investigate if impaired capacitation is associated with poor sperm motility, we assessed both PKA activity and the phosphorylation status of tyrosine residues, as hallmarks of the capacitation process. According to this analysis, there were no apparent differences in the profile of PKA-

phosphorylated substrates (Fig. 5A) at either 10 min or 120 min of incubation in TYH medium. Furthermore, we did not observe any clear differences in phosphorylation of tyrosine residues by western blotting (Fig. 5B). This was confirmed by immunostaining for tyrosine residue phosphorylation (Fig. 5C); although the *Cabyr*-KO spermatozoa did seem to exhibit weaker signals, the difference between fertile heterozygous samples and severely subfertile homozygous samples was not significant at any time point investigated (Fig. 5D). These results suggest that CABYR is not absolutely necessary for PKA substrate phosphorylation and subsequent phosphorylation of tyrosine residues.

Fibrous sheath integrity

To investigate the cause of the motility defect, we examined the ultrastructure of mature cauda epididymal spermatozoa (Fig. 6A–F). As a result of transmission electron microscopic analysis, we found that the fibrous sheath was specifically disorganized in the *Cabyr*-KO spermatozoa with fibres unwound and increased cytosolic space between the axoneme and the plasma membrane (Fig. 6B). Further analysis of cross sections of the principal piece revealed that the transverse ribs of the fibrous sheath were preferentially disrupted or expanded and that these were significantly different to those of controls ($P<0.05$; Fig. 6C and D). In contrast, the fibrous sheath adjacent to doublet microtubules 3 and 8, where the longitudinal columns of the fibrous sheath are located (Eddy et al., 2003), was not missing; however, it should be noted that the structure did not seem to be normal compared to that of the control (Fig. 6C). Also, in the medial section of longitudinally lying flagella, containing ribs or longitudinal columns, the disruptions were observed in the ribs but not in the longitudinal columns (0 out of 22 flagella examined; Fig. S3A). Such abnormalities of the fibrous sheath ribs were further
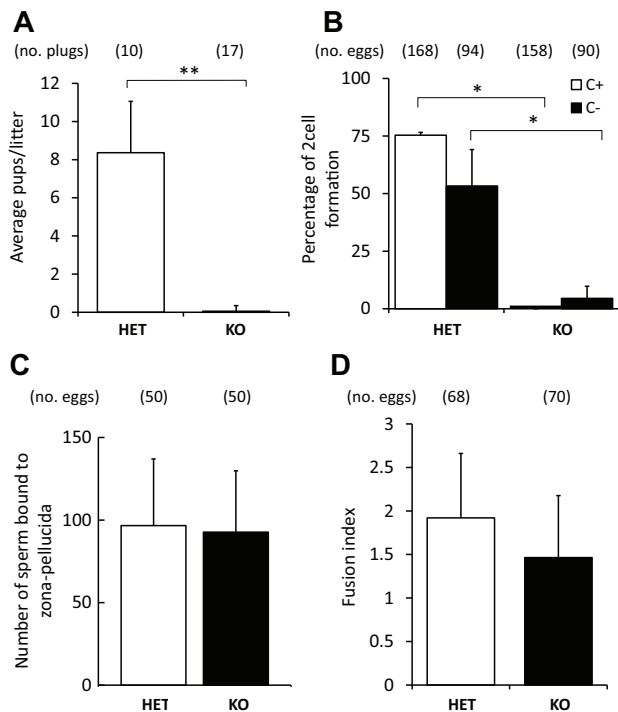
Fig. 3. Fertility analysis of *Cabyr*-KO mice. (A) Litter size is shown as the number of pups per litter, two WT females were caged with each male. The average litter size was 8.4±2.7 vs 0.06±0.3 (HET versus KO; mean±s.d.). The number of plugs counted is shown above the graph. (B) IVF using cumulus-intact (C+) and cumulus-free (C−) oocytes. The average percentages of oocytes that reached the two-cell stage when incubated with HET or KO spermatozoa were (mean±s.d.): C+, 75.4%±14.0 vs 0%±0 (HET versus KO); C−, 53.3%±15.8 vs 4.9%±5.3 (HET versus KO). The number of oocytes analyzed is shown above the graph. Black line above *x*-axis (KO, C+) indicates zero fertilized oocytes. (C) The zona-pellucida-binding assay is represented by the number of spermatozoa bound to the zona pellucida of WT oocytes, 97±40 vs 93±37 (HET versus KO). The number of oocytes analyzed is shown above graph. (D) Zona-pellucida-free fusion is represented by the fusion index, which was 1.92±0.74 vs 1.46±0.71 (HET versus KO; mean±s.d.). The number of oocytes analyzed is shown above graph. Fusion index, fused spermatozoa per oocyte. Each experiment used three HET and three KO males. *$P<0.05$, **$P<0.01$ (Student's *t*-test). Error bars are mean±s.d.

confirmed by a significantly higher frequency of vertically aligned ribs in the lateral sections of longitudinally lying flagella (Fig. S3B,C).

In addition to the abnormalities in the fibrous sheath, the disorganized axonemal structure in both the proximal and distal regions of the principal piece were observed in *Cabyr*-KO spermatozoa (black arrows in Fig. 6C). These abnormalities, defined as more or fewer doublet microtubules than in the 9+2 organization of the axoneme, tended to be more frequent in the distal region of KO spermatozoa compared to in the same region of controls, and the number of abnormalities increased along the length (Fig. 6E; Fig. S4). Occasionally, we observed an increased tendency of extra doublet microtubules located outside of the fibrous sheath to form (white arrows in Fig. 6C,F). In contrast, no structural abnormalities were observed in the midpiece (Fig. 6E), suggesting that the microtubule extension from the centriole occurs normally, even in *Cabyr*-KO mice.

DISCUSSION

This study utilized the CRISPR–Cas9 genetic manipulation technology to knockout *Cabyr* in mice. The N-terminus of the protein (the second exon) was targeted successfully, and homozygous

Cabyr-KO mice were severely subfertile. Although there were no problems with zona-pellucida binding or fusion with the plasma membrane of the egg in IVF, there were significant defects in the motility of *Cabyr*-KO spermatozoa that could cause impaired zona pellucida penetration. The fibrous sheath of the *Cabyr*-KO spermatozoa was severely disrupted, and the organization of the axoneme in the principal piece of the flagellum was clearly compromised. These data indicate that CABYR is an essential structural component of the fibrous sheath and that abnormal fibrous sheath formation in the *Cabyr*-KO spermatozoa leads to impaired sperm motility and severe male subfertility. It would be interesting to analyze if Ca^{2+}-binding and/or phosphorylated properties of CABYR are involved in the formation of the fibrous sheath. This could be done by mutating specific regions of CABYR with the CRISPR–Cas9 system (Wang et al., 2013; Young et al., 2015).

There are several proteins that have been identified that are localized in the fibrous sheath. Apart from AKAP3 and AKAP4, the other most notable of these are the proteins containing an R2D2 domain. CABYR is one of four proteins known to have this domain. Knockout studies analysing two more of these proteins, Ropporin 1 (ROPN1), as well as a similar protein, Ropporin1-like (ROPN1L), indicated defects in the integrity of the fibrous sheath (double KO) exhibiting thinning of the principal piece and a loss of AKAP3 (Fiedler et al., 2013). Unfortunately, there was no further investigation of the ultrastructure of these spermatozoa so it is unclear whether the integrity of the fibrous sheath remained intact. The *Ropn1 Ropn1l* double KO mouse line exhibits a complete failure in fertilization (Fiedler et al., 2013). The fourth R2D2-domain-containing protein, SPA17 has not yet been knocked out, although it too can bind to AKAP3 (Lea et al., 2004) and is localized to the fibrous sheath (Chiriva-Internati et al., 2009), indicating that knockout might potentially result in a phenotype similar to that upon loss of CABYR. Combined with our current data on CABYR, it appears that at least three of the four proteins containing the R2D2 domain appear to be essential for the correct formation of a fibrous sheath.

In addition to the proteins containing the R2D2 domain, the protein fibrous sheath CABYR binding (FSCB) is localized in the fibrous sheath and interacts with ROPN1 and ROPN1L (Zhang et al., 2016). As the name suggests, FSCB binds directly to CABYR (Li et al., 2007), and research has shown that it is phosphorylated by PKA and that it binds to Ca^{2+}, placing it firmly in the centre of sperm motility pathways (Liu et al., 2011; Zhang et al., 2016). In light of the findings of this research, FSCB would be a very promising candidate for future research, and with the speed and ease of the CRISPR–Cas9 system, it should not take too long to discover the function *in vivo*.

One of the important proteins within the fibrous sheath is AKAP4. Given that CABYR resides in the fibrous sheath, it stands to reason that a reduction in AKAP4 could also help to explain the lack of motility. Indeed, when *Akap4* is knocked out, there is a large reduction in the size and integrity of the fibrous sheath (Miki et al., 2002), which is similar to that seen in the *Cabyr*-KO mice. However, motility of the *Akap4*-KO spermatozoa was more severely compromised than that seen in the *Cabyr*-KO spermatozoa, with no forward progressive motility and less than 10% of spermatozoa showing any motility (Miki et al., 2002). In addition, *Akap4*-KO spermatozoa exhibited shortened flagellum, and the end piece was sometimes curled or splayed apart into fine filaments (Miki et al., 2002). In our analysis, we saw no effect on AKAP4 in terms of the amount of protein present (Fig. 2D). In addition, although AKAP4 undergoes PKA-dependent phosphorylation on serine and tyrosine residues, the lack of CABYR did not appear to impact on these
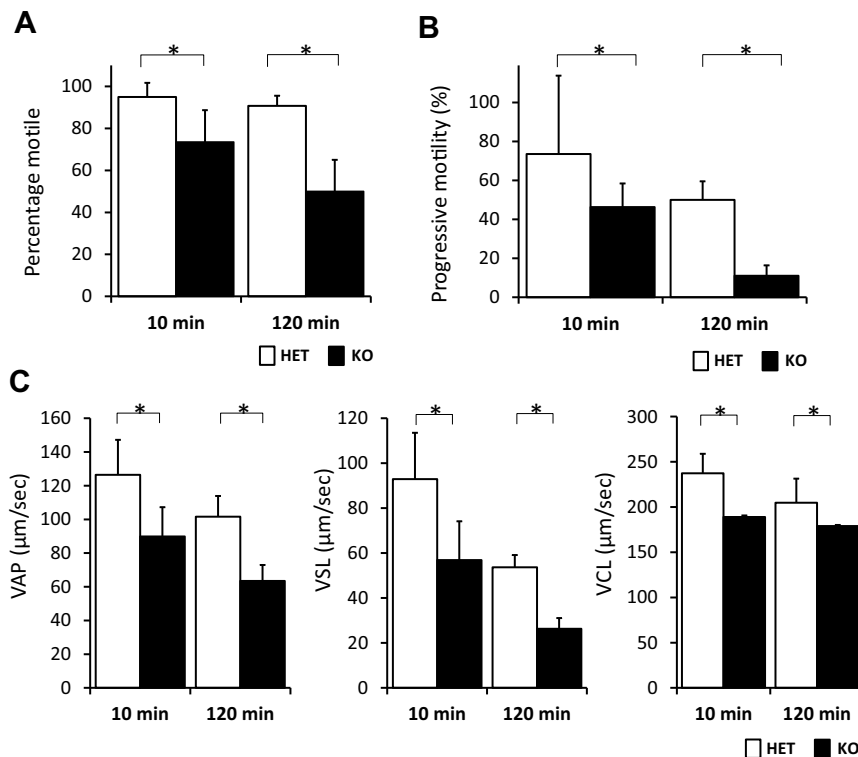
Fig. 4. Motility analysis of *Cabyr*-KO mice.
(A) Percentage of spermatozoa showing motility (total motility), (B) percentage of spermatozoa showing forward movement (progressive motility) and (C) CASA motility parameters; (left to right) average path velocity (VAP), straight line velocity (VSL), curvilinear velocity (VCL). Spermatozoa were incubated in capacitation medium (TYH) and motility measured at 10 min (un-capacitated) and 120 min (capacitated) to assess motility before and after capacitation. Three males for HET and three males for KO. More than 200 spermatozoa were analyzed for each male. *$P<0.05$ (Student's t-test). Error bars are mean±s.d.

signalling pathways. Therefore, these results suggest that CABYR is not necessary for the correct organization of AKAP4.

Previous work has indicated that CABYR is localized to the fibrous sheath, over its entire surface, including the inner and outer surfaces of the ribs and LCs (Naaby-Hansen et al., 2002; Kim et al., 2005). Our study revealed that disrupted structures were observed in the ribs but not in the longitudinal columns (Fig. 6; Fig. S3). It has been reported that the longitudinal columns are formed before the ribs (Sakai et al., 1986), and loss of CABYR from the cytoplasm occurs slightly later than AKAP4, a major component of the entire fibrous sheath (Li et al., 2010). Combining these facts together indicates that CABYR is involved in a step of rib formation and/or stabilization that occurs after basic organization of the longitudinal columns has been established.

One of the most fascinating features of the *Cabyr*-KO spermatozoa was the incorrect doublet microtubule localization (Fig. 6C–F). However, although we observed displacement of the doublet microtubules, the accessory components (including the outer and inner dynein arms or radial spokes) of these doublet microtubules, as well as those in central pair apparatus, appeared to have normal morphology. In another animal model, the *enolase 4* (*Eno4*)-KO mouse, impairment of the fibrous sheath has been noted (Nakamura et al., 2013), and the *Eno4*-KO mice also showed disrupted axonemes; however, no statistical analysis was given for that and additional doublet microtubules outside the fibrous sheath have not been described (Nakamura et al., 2013). Thus, given both the *Cabyr*- and *Eno4*-KO mice display poor fibrous sheath formation and lack (or, in the case of *Cabyr*-KO, show additional) doublet microtubules, we suggest that the correct formation of the fibrous sheath is important for axoneme placement or stability. In contrast, no abnormalities were observed in the axoneme of *Akap4*-KO spermatozoa. These results suggest that the integration of CABYR into the fibrous sheath is necessary for the proper formation and/or maintenance of the axoneme, but not AKAP4. Without the correct

formation of these essential structures (fibrous sheath and/or axoneme), the *Cabyr*-KO spermatozoa have poor progressive motility, severely reducing their fertilizing ability.

Given the uniqueness of this model, we questioned whether a lack of CABYR possibly accounts for a failure of fertilization in humans. Male factor infertility is very common, affecting 1 in 20 men of reproductive age (Aitken et al., 2014). However, the precise mechanisms underlying defects are still unknown and are likely to involve several genes. In one case study, two men have been reported to have defects in the fibrous sheath of their spermatozoa (Escalier and Albert, 2006). Much like our *Cabyr* model, normal sperm motility in both of these men was extremely low (5% and <5%, respectively) (Escalier and Albert, 2006). Of particular note, the transmission electron microscopy analysis of their sperm flagella demonstrated that additional axonemal microtubules were present unusually between the plasma membrane and the fibrous sheath, very much like that seen in the *Cabyr* model. Another study has found the expression of a testis-specific isoform of CABYR to be greatly reduced in asthenozoospermic (impaired motility) men (Shen et al., 2015). Hence, it is plausible that a defect in or a lack of CABYR underpins some forms of human male infertility.

MATERIALS AND METHODS
Animals
All animal experiments were approved by the Animal Care and Use committee of the Research Institute for Microbial Diseases, Osaka University.

Off-target analysis
Potential off-target sites were found using free software, Bowtie (http://bowtie-bio.sourceforge.net/index.shtml), with rules that have been outlined previously (Mali et al., 2013; Wang et al., 2013; Yang et al., 2013). Twelve to 14 bases preceding the protospacer adjacent motif (PAM) sequence with AGG, GGG, CGG and TGG were aligned with the mouse genome (mm9; University of California Santa Cruz). sgRNAs with fewer off-target sites were designed.
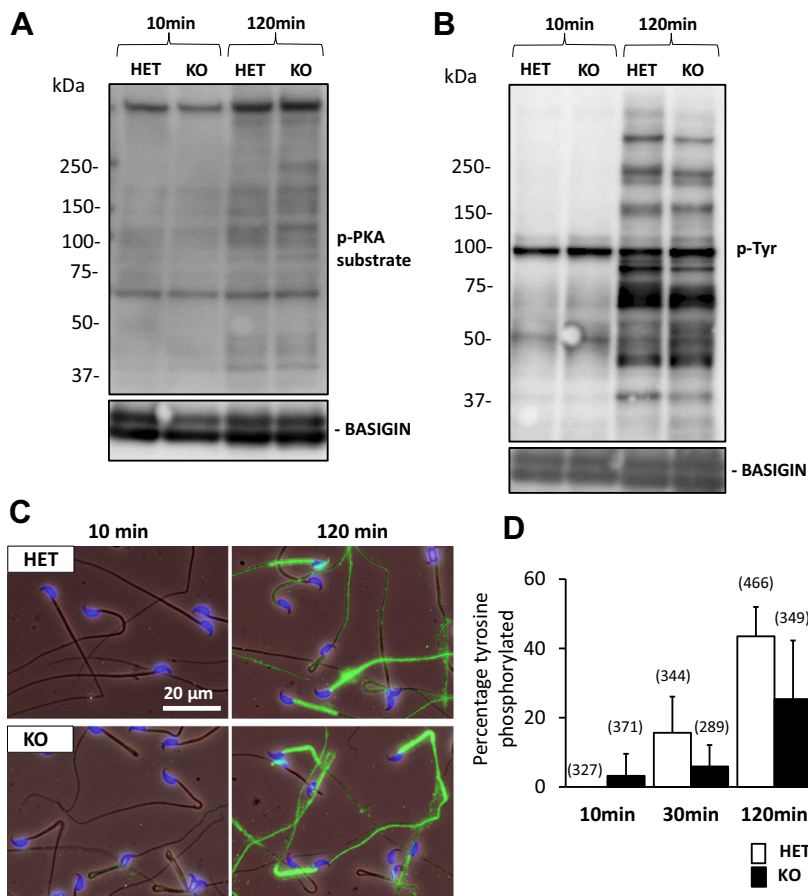
Fig. 5. Analysis of phosphorylated PKA substrates and phosphorylated tyrosine residues. (A) Immunoblot of phosphorylated PKA substrates (p-PKA substrate). Spermatozoa were incubated in capacitation medium (TYH) and proteins were extracted from the spermatozoa at 10 min (un-capacitated) and 120 min to assess changes in p-PKA substrate. (B) Immunoblot of phosphorylated tyrosine residues (p-Tyr) in un-capacitated (10 min) versus capacitated (120 min) spermatozoa. (C) Immunolocalization of phosphorylated tyrosine residues in un-capacitated (10 min) versus capacitated (120 min) spermatozoa. Green, tyrosine phosphorylation; blue, nuclear staining. (D) Counts of strong phosphorylated tyrosine residue signals at the indicated time points over a 120-min incubation in TYH medium. We analyzed the spermatozoa from four HET and four KO males. The total number of spermatozoa examined is shown above the graph. Error bars are mean±s.d.

Plasmid and oligonucleotide preparation

The plasmids expressing hCas9 and sgRNA were prepared by ligating oligonucleotides into the BbsI site of pX330 (http://www.addgene.org/42230/; Cong et al., 2013). The pCAG-EGxxFP target plasmid was prepared as previously described (http://www.addgene.org/50716/; Mashiko et al., 2013). The sgRNA sequence target was 5′-GGCCTCAAGACTCTGCTT-GA-3′ (sgRNA1).

sgRNA validation assay

Validation of sgRNA (CRISPR) cleavage activity was performed by transfecting HEK293T cells, as previously reported (Mashiko et al., 2013).

Pronuclear injection

B6D2F1 female mice were induced to superovulate and mated with B6D2F1 males, and fertilized eggs were collected from the oviduct. The pX330 plasmids were injected into one of the pronuclei at 5 ng/µl. The injected eggs were cultivated in potassium simplex optimization medium (kSOM) (Ho et al., 1995) overnight, then two-cell stage embryos were transferred into the oviducts of pseudopregnant ICR females. The pups obtained were genotyped by performing PCR and subsequent sequence analysis.

Genotyping of subsequent generations

PCR analysis of genomic DNA was performed for *Cabyr* using the following primer sets: *Cabyr* forward (plus EcoRV restriction enzyme sequence) 5′-AAGATATCTGTGCATTAGTAAGCAGTGG-3′, reverse (plus BamHI restriction enzyme sequence) 5′-AAGGATCCTGACGA-CCCTGCTGAAGTGG-3′. Direct sequencing of PCR products was then performed. Restriction enzyme sites were added because these primers were used for pCAG-EGxxFP plasmid construction. The *Cabyr*[+17] allele had an insertion of the HindIII site, allowing for fast analysis of the genotype by PCR and subsequent enzyme digestion.

Intracytoplasmic sperm injection

ICSI was performed as previously reported (Inoue et al., 2005). In brief, mature oocytes were collected from superovulated B6D2F1 mice 13–15 h after injection of human chorionic gonadotropin. After hyaluronidase treatment to remove the cumulus oocyte complex, oocytes were placed in fresh Chatot, Ziomek and Bavister (CZB) medium at 37°C under 5% CO_2 in air until subjected to ICSI. Each sperm head was separated from the tail by applying a few piezo pulses, then injected into an oocyte using a piezo manipulator (PrimeTech, Ibaraki, Japan) (Kimura and Yanagimachi, 1995). The next day, two-cell embryos were counted and transferred to pseudopregnant females. Pups were genotyped at birth.

In vivo and in vitro male fertility tests

Sexually matured *Cabyr*-KO male mice were caged with 2-month-old B6D2F1 female mice for 3 months, and the number of pups was counted at the day of birth. IVF analysis was performed as previously reported (Inoue et al., 2005).

For zona-pellucida-binding assessment, the cumulus layer was removed from the oocytes through treatment with 330 µg/ml hyaluronidase (Sigma-Aldrich). The cumulus-free oocytes were incubated with $2×10^5$ spermatozoa/ml for 30 min at 37°C under 5% CO_2. Cells were then treated with 0.04% paraformaldehyde to halt sperm movement and observed under a differential interference contrast microscope. To count the number of spermatozoa that had bound to the zona pellucida, the sperm heads were stained with Hoechst 33342 nuclear stain and observed under a fluorescence microscope (excitation with ultraviolet light).

The zona-pellucida-free fusion assay was performed as previously reported (Inoue et al., 2005), with some minor changes. In brief, the zona pellucida was removed using 1 mg/ml collagenase (Sigma-Aldrich). Zona-pellucida-free oocytes were then pre-loaded with Hoechst 33342 through incubation in TYH medium containing the dye (1 µg/ml) for 10 min, then washed thoroughly. Spermatozoa were added to a concentration of $2×10^5$
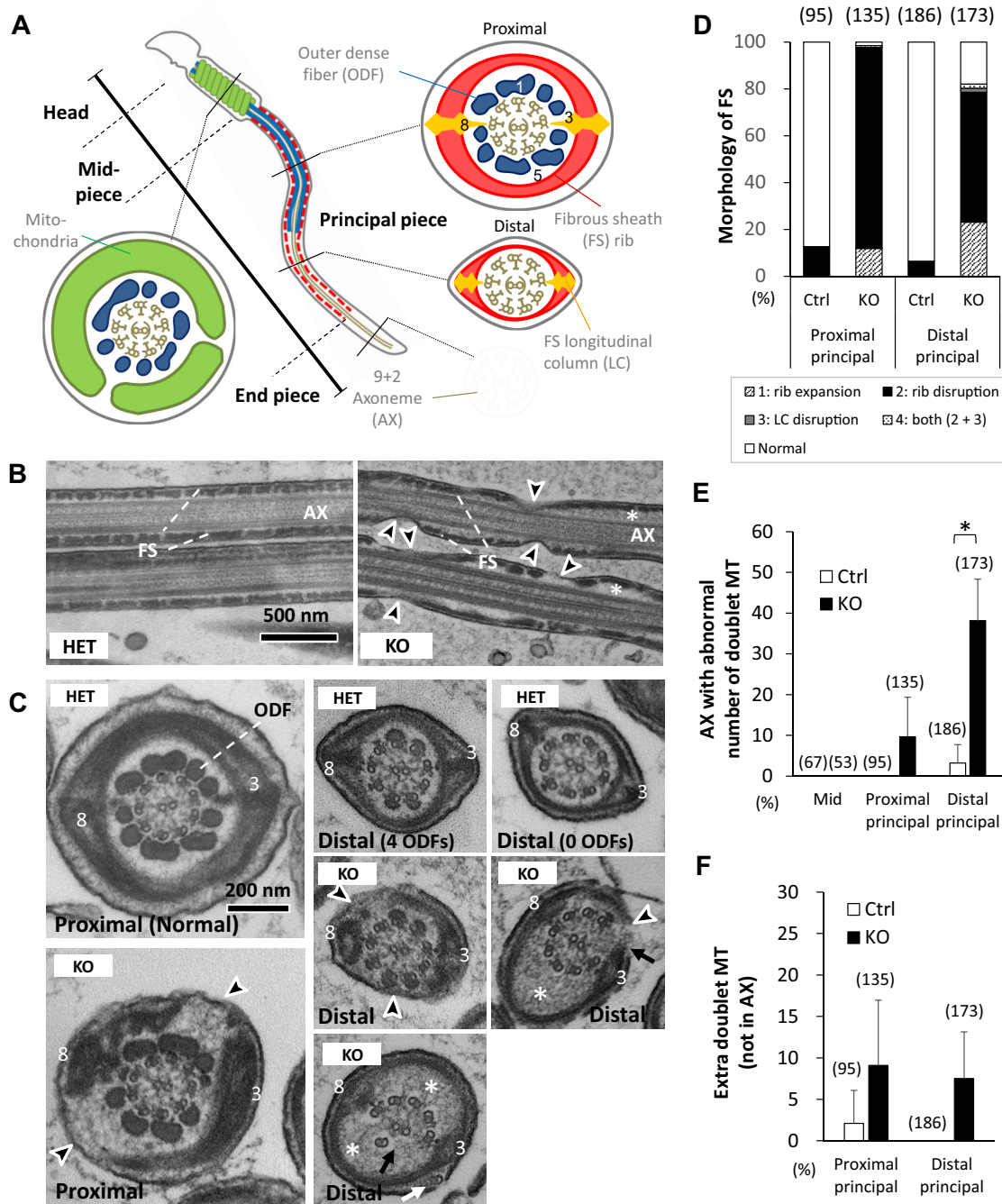
Fig. 6. Ultrastructural analysis of the flagellum of *Cabyr*-KO cauda epididymal spermatozoa. (A) Schematic drawing of the internal structure of mature mouse spermatozoon. Proximal and distal regions of the principal piece were defined as having 5–9 and 0–4 outer dense fibres, respectively. Longitudinal columns are located adjacent to doublet microtubules 3 and 8 (indicated in the cross section of the proximal principal piece). (B) Longitudinal view and (C) cross section of a principal piece. Black arrowheads indicate disrupted fibrous sheaths (FSs). White asterisks indicate expanded cytosolic regions. Black arrows indicate absence of doublet microtubules. White arrows indicate extra double microtubules outside of the fibrous sheath. Doublet microtubules 3 and 8 are indicated. (D) Quantification of the morphological analysis of fibrous sheaths. There were significant differences between control and KO with regards to expanded ribs, disrupted ribs and normal fibrous sheath at both proximal and distal regions (*P*<0.05, Student's *t*-test). WT and HET were used as Ctrl. (E) Quantification of abnormal axonemal structures (AX). Abnormal axonemes were defined as having more or fewer than nine doublet microtubules (MTs). **P*<0.05 (Student's *t*-test). (F) Analysis of axonemes with extra doublet microtubules. The number of flagellar sections analyzed are shown above the graph. Error bars are mean±s.d.

spermatozoa/ml. After 30 min of incubation, the eggs were fixed with 0.25% glutaraldehyde then observed under a fluorescence microscope (excitation with ultraviolet light).

Immunoblot analysis

Immunoblot analysis was performed as described previously (Inoue et al., 2008). Samples were subjected to sodium dodecyl sulphate polyacrylamide

gel electrophoresis (SDS-PAGE) under reduced conditions followed by western blotting. For CABYR staining, anti-CABYR polyclonal antibody (1/200, 12351-1-AP, ProteinTech); for phosphorylated tyrosines, anti-phosphorylated-tyrosine antibody clone 4G10®, horseradish peroxidase (HRP) conjugate (1/2000, 16-105, Merck Millipore); for phosphorylated PKA substrates, P-PKA-substrate RRXS/T antibody (1/1000, 100G7E, Cell Signaling); for AKAP3, anti-AKAP3 polyclonal antibody (1/1000, 13907-1-

AP, ProteinTech); for AKAP4, anti-AKAP82 monoclonal antibody (1/5000, 611564, BD Transduction Laboratories). Immunoreactive proteins were detected by using an ECL western blotting detection kit (GE Healthcare).

Immunolocalization of CABYR

The spermatozoa that had been prepared from cauda epididymis were incubated in a drop of TYH medium for 2 h at 37°C under 5% CO_2 and then spotted onto slides, air dried, fixed with 4% paraformaldehyde for 5 min and washed in PBS for 5 min. Nonspecific-protein-binding sites were blocked with 5% bovine serum albumin (BSA) in PBS with 0.1% Tween 20 at room temperature for 1 h. The slides were then incubated with anti-CABYR antibody (as above) or anti phosphotyrosine 4G10® Platinum (1/200, 05-1050X, Millipore) at 4°C overnight. Next, slides were incubated in the dark with Alexa-Fluor-488-conjugated anti-rabbit IgG (for CABYR) or anti-mouse IgG (for phosphorylated tyrosines) (Invitrogen) at room temperature in 5% BSA in PBS with 0.1% Tween 20. After being washed, the slides were mounted in PBS. The stained cells were observed under a fluorescence microscope. A FV-OSR system (Olympus, Tokyo, Japan) was used for super-resolution microscopy.

Acrosome reaction

To assess spontaneous acrosome reaction rates, the spermatozoa that had been prepared from cauda epididymis were incubated in a drop of TYH medium for 2 h at 37°C under 5% CO_2 and then spotted onto slides, air dried, fixed with 4% paraformaldehyde for 10 min and washed in PBS for 5 min. Nonspecific-protein-binding sites were blocked with 5% BSA in PBS with 0.1% Tween 20 at room temperature for 1 h. The slides were then incubated at 4°C overnight with anti-IZUMO1 antibody that was established in our laboratory (1/500, #125, Ikawa et al., 2011). Next, slides were incubated in the dark with Alexa-Fluor-488-conjugated anti-rat IgG (Invitrogen) at room temperature in 5% BSA in PBS with 0.1% Tween 20. After being washed, the slides were mounted in PBS containing Hoechst 33342 nuclear stain. The stained cells were observed under a fluorescence microscope. The acrosome reaction rate was calculated by counting the percentage of cells displaying IZUMO1 located throughout the complete sperm head, indicating the acrosome reaction had taken place.

Sperm motility analysis

Spermatozoa were collected from the cauda epididymis and suspended in TYH or non-capacitating medium (Chávez et al., 2012). Sperm motility was then measured using the CEROS sperm analysis system (software version 12.3; Hamilton Thorne Biosciences, Beverly, MA). The analysis setting described previously (Goodson et al., 2011) was used. Sperm motility was also analyzed with an Olympus BX-53 microscope equipped with a high-speed camera (HAS-L1, Ditect, Tokyo, Japan). Hyperactivated cells were counted as those showing the classic figure eight movement after 10 min and 120 min of incubation in TYH medium.

Electron microscopy analysis of the fibrous sheath

For ultrastructural analysis of sperm flagella, cauda epididymal samples were prepared for transmission electron microscopy analysis as previously described (Inoue et al., 2011b). One wild-type and two heterozygous males were examined as control group, whereas the KO group contained three KO males. All males were matured, and it should be noted that no difference was observed between wild-type and heterozygous spermatozoa. Ultrathin sections were prepared with a thickness of 70 nm and then examined using a JEM-1011 electron microscope (JEOL) at 80 kV. For the quantification of vertically aligned fibrous sheath ribs in lateral–longitudinal sections of principal pieces, flagella sections longer than 3 µm were examined whether they contained vertically aligned ribs or not. Numbering of doublet microtubules and evaluation of flagellar internal structures was performed as previously described (Nakamura et al., 2013).

Statistical analysis

Statistical analyses were performed using Student's t-test. Differences were considered significant at $P<0.05$ (*) or highly significant at $P<0.01$ (**) and $P<0.001$ (***). Error bars are s.d.

References

Aitken, R. J., Smith, T. B., Jobling, M. S., Baker, M. A. and De Iuliis, G. N. (2014). Oxidative stress and male reproductive health. *Asian J. Androl.* **16**, 31-38.

Bunch, D. O., Welch, J. E., Magyar, P. L., Eddy, E. M. and O'Brien, D. A. (1998). Glyceraldehyde 3-phosphate dehydrogenase-S protein distribution during mouse spermatogenesis. *Biol. Reprod.* **58**, 834-841.

Chávez, J. C., Hernández-González, E. O., Wertheimer, E., Visconti, P. E., Darszon, A. and Treviño, C. L. (2012). Participation of the Cl-/HCO(3)-exchangers SLC26A3 and SLC26A6, the Cl- channel CFTR, and the regulatory factor SLC9A3R1 in mouse sperm capacitation. *Biol. Reprod.* **86**, 1-14.

Chiriva-Internati, M., Gagliano, N., Donetti, E., Costa, F., Grizzi, F., Franceschini, B., Albani, E., Levi-Setti, P. E., Gioia, M., Jenkins, M. et al. (2009). Sperm protein 17 is expressed in the sperm fibrous sheath. *J. Transl. Med.* **7**, 61.

Colledge, M. and Scott, J. D. (1999). AKAPs: from structure to function. *Trends Cell Biol.* **9**, 216-221.

Cong, L., Ran, F. A., Cox, D., Lin, S., Barretto, R., Habib, N., Hsu, P. D., Wu, X., Jiang, W., Marraffini, L. A. et al. (2013). Multiplex genome engineering using CRISPR/Cas systems. *Science* **339**, 819-823.

Eddy, E. M., Toshimori, K. and O'brien, D. A. (2003). Fibrous sheath of mammalian spermatozoa. *Microsc. Res. Tech.* **61**, 103-115.

Escalier, D. and Albert, M. (2006). New fibrous sheath anomaly in spermatozoa of men with consanguinity. *Fertil. Steril.* **86**, 219.e1-219.e9.

Feiden, S., Stypa, H., Wolfrum, U., Wegener, G. and Kamp, G. (2007). A novel pyruvate kinase (PK-S) from boar spermatozoa is localized at the fibrous sheath and the acrosome. *Reproduction* **134**, 81-95.

Ficarro, S., Chertihin, O., Westbrook, V. A., White, F., Jayes, F., Kalab, P., Marto, J. A., Shabanowitz, J., Herr, J. C., Hunt, D. F. et al. (2003). Phosphoproteome analysis of capacitated human sperm: evidence of tyrosine phosphorylation of a kinase-anchoring protein 3 and valosin-containing protein/p97 during capacitation. *J. Biol. Chem.* **278**, 11579-11589.

Fiedler, S. E., Dudiki, T., Vijayaraghavan, S. and Carr, D. W. (2013). Loss of R2D2 Proteins ROPN1 and ROPN1L Causes Defects in Murine Sperm Motility, Phosphorylation, and Fibrous Sheath Integrity. *Biol. Reprod.* **88**, 41.

Fujihara, Y., Okabe, M. and Ikawa, M. (2014). GPI-anchored protein complex, LY6K/TEX101, is required for sperm migration into the oviduct and male fertility in mice. *Biol. Reprod.* **90**, 60.

Goodson, S. G., Zhang, Z., Tsuruta, J. K., Wang, W. and O'Brien, D. A. (2011). Classification of mouse sperm motility patterns using an automated multiclass support vector machines model. *Biol. Reprod.* **84**, 1207-1215.

Hanlon Newell, A. E., Fiedler, S. E., Ruan, J. M., Pan, J., Wang, P. J., Deininger, J., Corless, C. L. and Carr, D. W. (2008). Protein kinase A RII-like (R2D2) proteins exhibit differential localization and AKAP interaction. *Cell Motil. Cytoskelet.* **65**, 539-552.

Ho, H.-C. and Suarez, S. S. (2003). Characterization of the intracellular calcium store at the base of the sperm flagellum that regulates hyperactivated motility. *Biol. Reprod.* **68**, 1590-1596.

Ho, Y., Wigglesworth, K., Eppig, J. J. and Schultz, R. M. (1995). Preimplantation development of mouse embryos in KSOM: augmentation by amino acids and analysis of gene expression. *Mol. Reprod. Dev.* **41**, 232-238.

Ikawa, M., Inoue, N., Benham, A. M. and Okabe, M. (2010). Fertilization: a sperm's journey to and interaction with the oocyte. *J. Clin. Invest.* **120**, 984-994.

Ikawa, M., Tokuhiro, K., Yamaguchi, R., Benham, A. M., Tamura, T., Wada, I., Satouh, Y., Inoue, N. and Okabe, M. (2011). Calsperin is a testis-specific chaperone required for sperm fertility. *J. Biol. Chem.* **286**, 5639-5646.

Inoue, N., Ikawa, M., Isotani, A. and Okabe, M. (2005). The immunoglobulin superfamily protein Izumo is required for sperm to fuse with eggs. *Nature* **434**, 234-238.

Inoue, N., Ikawa, M. and Okabe, M. (2008). Putative sperm fusion protein IZUMO and the role of N-glycosylation. *Biochem. Biophys. Res. Commun.* **377**, 910-914.

Inoue, N., Ikawa, M. and Okabe, M. (2011a). The mechanism of sperm-egg interaction and the involvement of IZUMO1 in fusion. *Asian J. Androl.* **13**, 81-87.

Inoue, N., Satouh, Y., Ikawa, M., Okabe, M. and Yanagimachi, R. (2011b). Acrosome-reacted mouse spermatozoa recovered from the perivitelline space can fertilize other eggs. *Proc. Natl. Acad. Sci. USA* **108**, 20008-20011.

Kim, Y.-H., Jha, K. N., Mandal, A., Vanage, G., Farris, E., Snow, P. L., Klotz, K., Naaby-Hansen, S., Flickinger, C. J. and Herr, J. C. (2005). Translation and assembly of CABYR coding region B in fibrous sheath and restriction of calcium binding to coding region A. *Dev. Biol.* **286**, 46-56.

Kimura, Y. and Yanagimachi, R. (1995). Mouse oocytes injected with testicular spermatozoa or round spermatids can develop into normal offspring. *Development* **121**, 2397-2405.

Krisfalusi, M., Miki, K., Magyar, P. L. and O'Brien, D. A. (2006). Multiple glycolytic enzymes are tightly bound to the fibrous sheath of mouse spermatozoa. *Biol. Reprod.* **75**, 270-278.

Lea, I. A., Widgren, E. E. and O'Rand, M. G. (2004). Association of sperm protein 17 with A-kinase anchoring protein 3 in flagella. *Reprod. Biol. Endocrinol.* **2**, 57.

Li, Y.-F., He, W., Jha, K. N., Klotz, K., Kim, Y.-H., Mandal, A., Pulido, S., Digilio, L., Flickinger, C. J. and Herr, J. C. (2007). FSCB, a novel protein kinase A-phosphorylated calcium-binding protein, is a CABYR-binding partner involved in late steps of fibrous sheath biogenesis. *J. Biol. Chem.* **282**, 34104-34119.

Li, Y.-F., He, W., Kim, Y.-H., Mandal, A., Digilio, L., Klotz, K., Flickinger, C. J. and Herr, J. C. (2010). CABYR isoforms expressed in late steps of spermiogenesis bind with AKAPs and ropporin in mouse sperm fibrous sheath. *Reprod. Biol. Endocrinol.* **8**, 101.

Li, Y.-F., He, W., Mandal, A., Kim, Y.-H., Digilio, L., Klotz, K., Flickinger, C. J., Herr, J. C. and Herr, J. C. (2011). CABYR binds to AKAP3 and Ropporin in the human sperm fibrous sheath. *Asian J. Androl.* **13**, 266-274.

Liu, S.-L., Ni, B., Wang, X.-W., Huo, W.-Q., Zhang, J., Tian, Z.-Q., Huang, Z.-M., Tian, Y., Tang, J., Zheng, Y.-H. et al. (2011). FSCB phosphorylation in mouse spermatozoa capacitation. *BMB Rep.* **44**, 541-546.

Mali, P., Yang, L., Esvelt, K. M., Aach, J., Guell, M., Dicarlo, J. E., Norville, J. E. and Church, G. M. (2013). RNA-guided human genome engineering via Cas9. *Science* **339**, 823-826.

Mashiko, D., Fujihara, Y., Satouh, Y., Miyata, H., Isotani, A. and Ikawa, M. (2013). Generation of mutant mice by pronuclear injection of circular plasmid expressing Cas9 and single guided RNA. *Sci. Rep.* **3**, 3355.

Meistrich, M. L., Mohapatra, B., Shirley, C. R. and Zhao, M. (2003). Roles of transition nuclear proteins in spermiogenesis. *Chromosoma* **111**, 483-488.

Miki, K., Willis, W. D., Brown, P. R., Goulding, E. H., Fulcher, K. D. and Eddy, E. M. (2002). Targeted disruption of the Akap4 gene causes defects in sperm flagellum and motility. *Dev. Biol.* **248**, 331-342.

Miyata, H., Satouh, Y., Mashiko, D., Muto, M., Nozawa, K., Shiba, K., Fujihara, Y., Isotani, A., Inaba, K. and Ikawa, M. (2015). Sperm calcineurin inhibition prevents mouse fertility with implications for male contraceptive. *Science* **350**, 442-445.

Naaby-Hansen, S., Mandal, A., Wolkowicz, M. J., Sen, B., Westbrook, V. A., Shetty, J., Coonrod, S. A., Klotz, K. L., Kim, Y.-H., Bush, L. A. et al. (2002). CABYR, a novel calcium-binding tyrosine phosphorylation-regulated fibrous sheath protein involved in capacitation. *Dev. Biol.* **242**, 236-254.

Nakamura, N., Dai, Q., Williams, J., Goulding, E. H., Willis, W. D., Brown, P. R. and Eddy, E. M. (2013). Disruption of a spermatogenic cell-specific mouse enolase 4 (eno4) gene causes sperm structural defects and male infertility. *Biol. Reprod.* **88**, 90.

Navarrete, F. A., García-Vázquez, F. A., Alvau, A., Escoffier, J., Krapf, D., Sánchez-Cárdenas, C., Salicioni, A. M., Darszon, A. and Visconti, P. E. (2015). Biphasic Role of Calcium in Mouse Sperm Capacitation Signaling Pathways. *J. Cell Physiol.* **230**, 1758-1769.

Okabe, M. (2013). The cell biology of mammalian fertilization. *Development* **140**, 4471-4479.

Sakai, Y., Koyama, Y.-I., Fujimoto, H., Nakamoto, T. and Yamashina, S. (1986). Immunocytochemical study on fibrous sheath formation in mouse spermiogenesis using a monoclonal antibody. *Anat. Rec.* **215**, 119-126.

Sen, B., Mandal, A., Wolkowicz, M. J., Kim, Y.-H., Reddi, P. P., Shetty, J., Bush, L. A., Flickinger, C. J. and Herr, J. C. (2003). Splicing in murine CABYR and its genomic structure. *Gene* **310**, 67-78.

Shen, S., Wang, J., Liang, J. and Zhu, C. (2015). Low-expressed testis-specific calcium-binding protein CBP86-IV (CABYR) is observed in idiopathic asthenozoospermia. *World J. Urol.* **33**, 633-638.

Suarez, S. S., Varosi, S. M. and Dai, X. (1993). Intracellular calcium increases with hyperactivation in intact, moving hamster sperm and oscillates with the flagellar beat cycle. *Proc. Natl. Acad. Sci. USA* **90**, 4660-4664.

Toyoda, Y., Yokoyama, M. and Hoshi, T. (1971). Studies on the fertilization of mouse eggs in vitro. *Jpn. J. Anim. Reprod.* **16**, 147-151.

Wang, H., Yang, H., Shivalila, C. S., Dawlaty, M. M., Cheng, A. W., Zhang, F. and Jaenisch, R. (2013). One-step generation of mice carrying mutations in multiple genes by CRISPR/Cas-mediated genome engineering. *Cell* **153**, 910-918.

Westhoff, D. and Kamp, G. (1997). Glyceraldehyde 3-phosphate dehydrogenase is bound to the fibrous sheath of mammalian spermatozoa. *J. Cell Sci.* **110**, 1821-1829.

Yanagimachi, R. (1994). *Mammalian Fertilization*. New York: Raven Press.

Yang, H., Wang, H., Shivalila, C. S., Cheng, A. W., Shi, L. and Jaenisch, R. (2013). One-step generation of mice carrying reporter and conditional alleles by CRISPR/Cas-mediated genome engineering. *Cell* **154**, 1370-1379.

Young, S. A., Miyata, H., Satouh, Y., Kato, H., Nozawa, K., Isotani, A., Aitken, R. J., Baker, M. and Ikawa, M. (2015). CRISPR/Cas9-mediated rapid generation of multiple mouse lines identified Ccdc63 as essential for spermiogenesis. *Int. J. Mol. Sci.* **16**, 24732-24750.

Zhang, X., Chen, M., Yu, R., Liu, B., Tian, Z. and Liu, S. (2016). FSCB phosphorylation regulates mouse spermatozoa capacitation through suppressing SUMOylation of ROPN1/ROPN1L. *Am. J. Transl. Res.* **8**, 2776-2782.
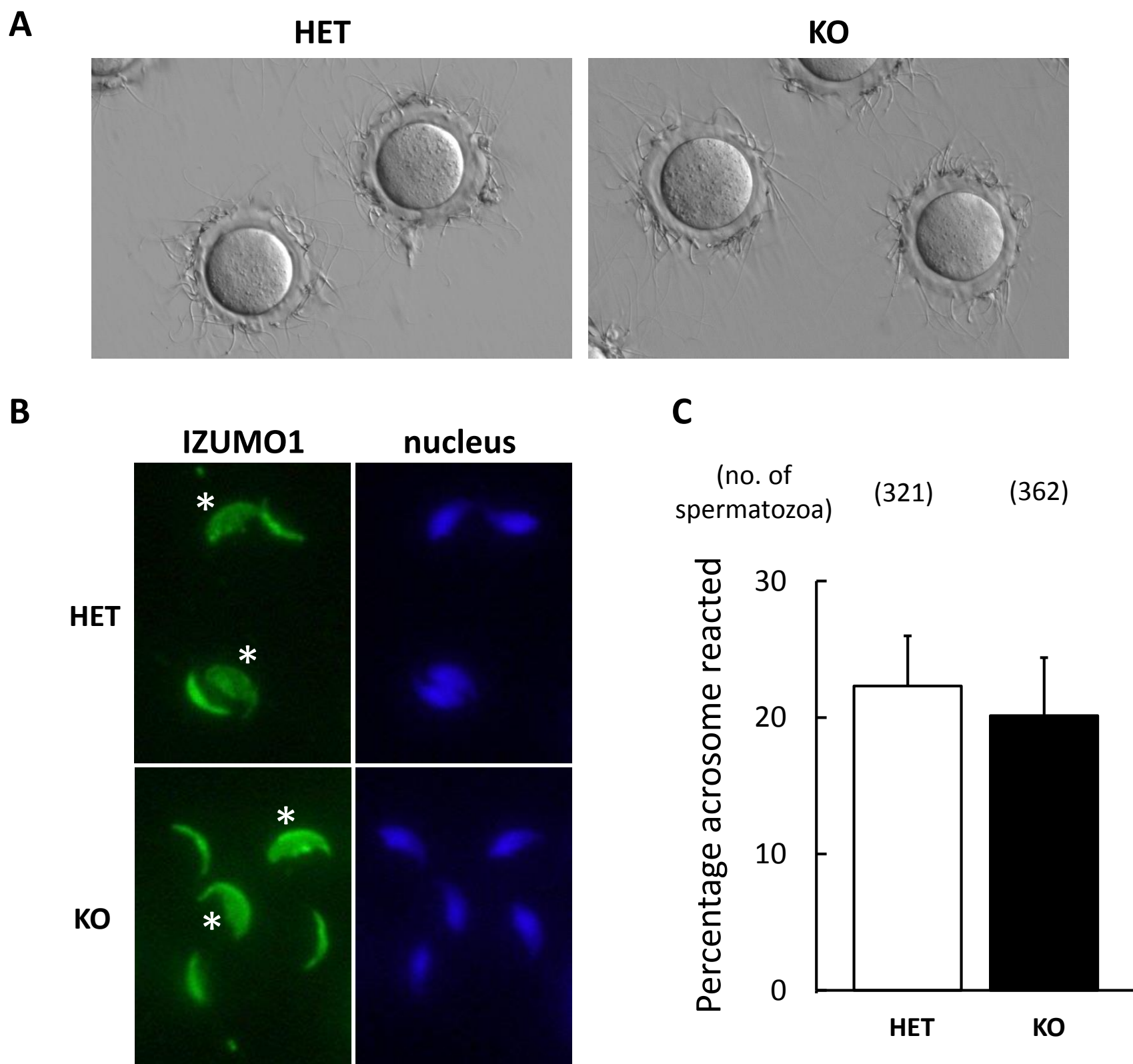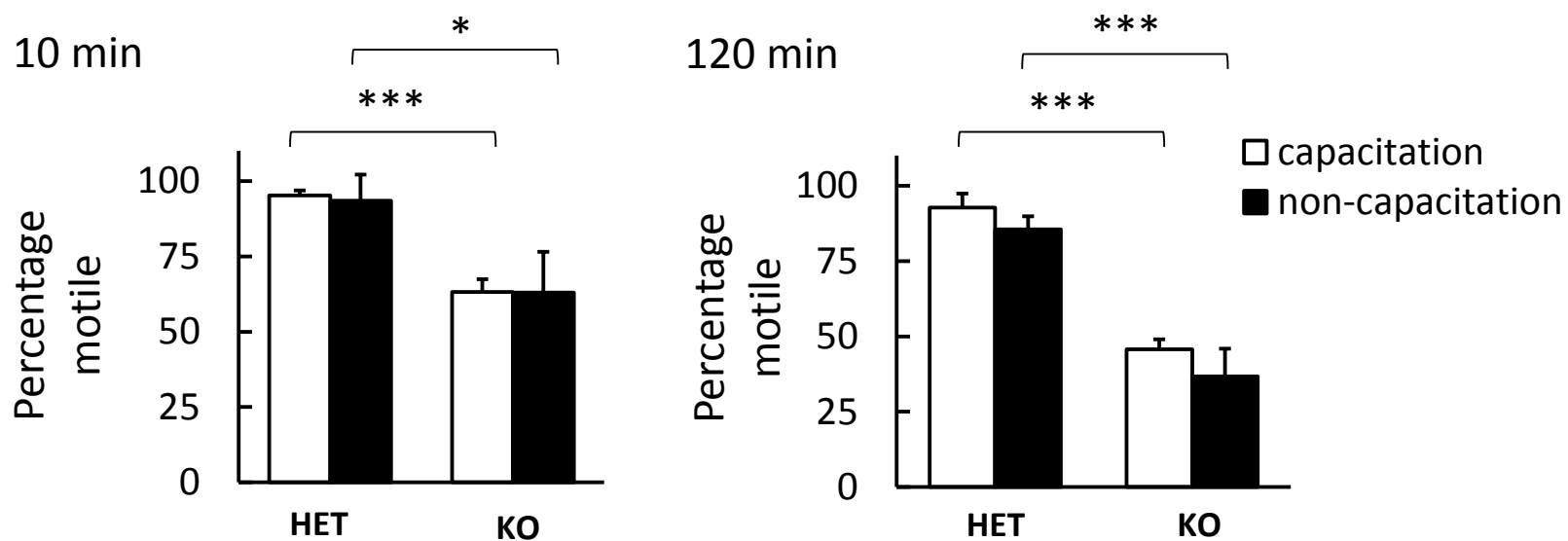
Fig. S1. Zona-binding ability and acrosome reaction of *Cabyr* KO spermatozoa. A) Differential interference contrast images of ZP binding. B) Immunostaining of IZUMO1 shows acrosome reacted (white asterisk) versus unreacted cells. C) Quantification of acrosome reacted spermatozoa. Number of spermatozoa counted is shown above graph.
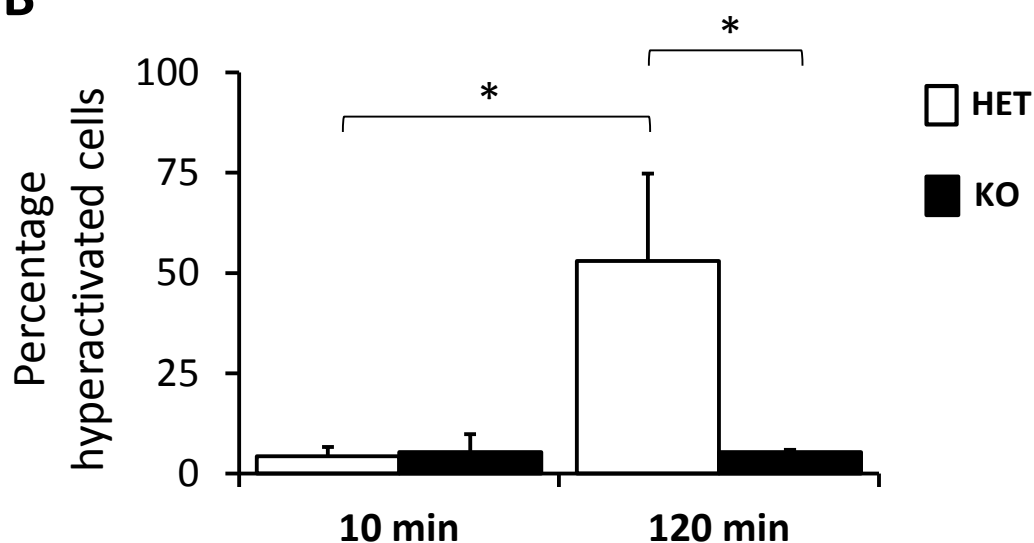
Fig. S2. Motility analysis of *Cabyr* KO spermatozoa. A) Motility of spermatozoa when incubated in capacitating and non-capacitating media. Males: 4 for HET and 4 for KO. More than 200 spermatozoa were analyzed for each male. B) Hyperactivation analysis of *Cabyr* KO spermatozoa. Males: 3 for HET and 3 for KO. 100 spermatozoa per male were assessed for hyperactivated motility.
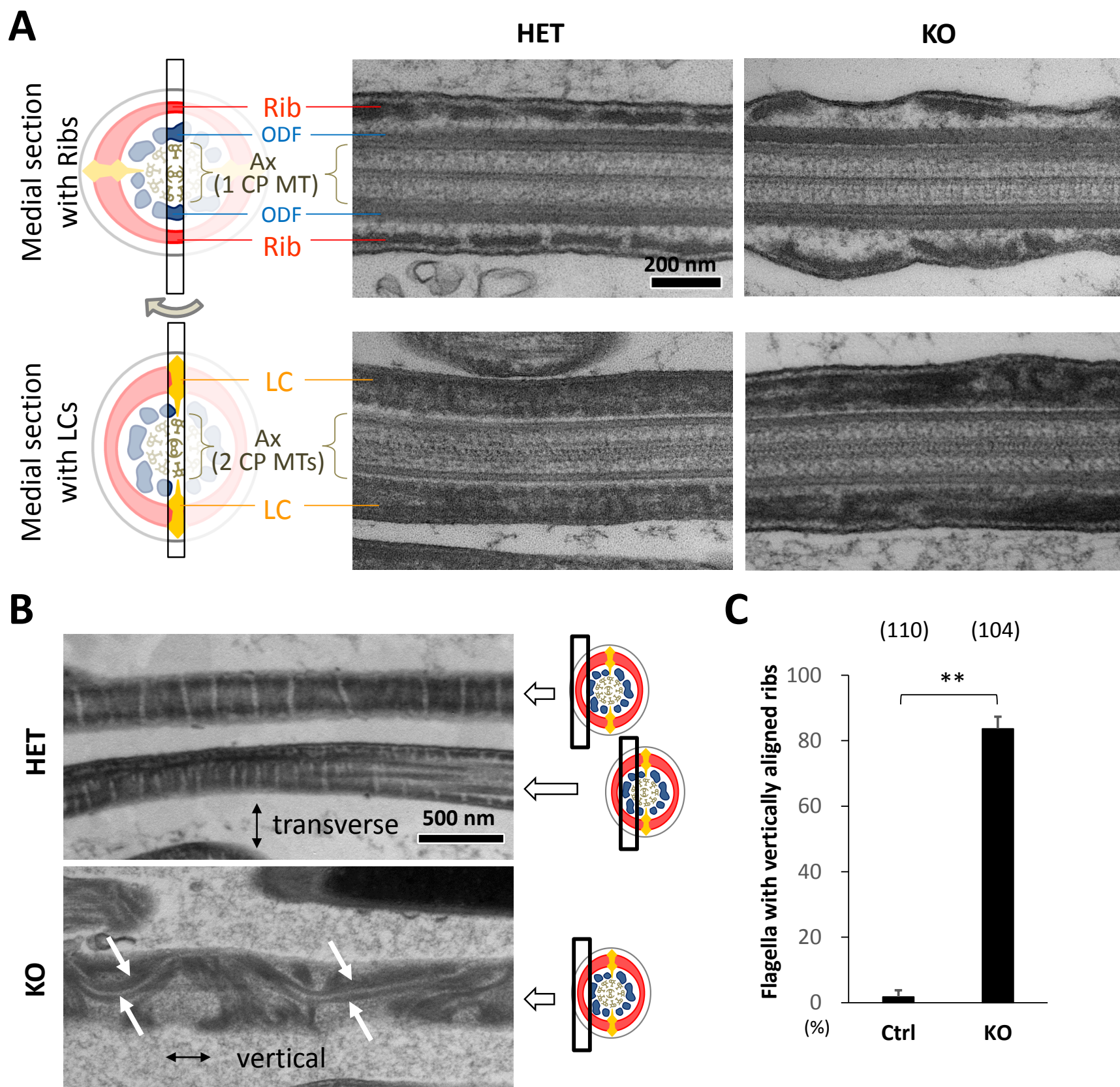
Fig. S3. Ultrastructural analysis for longitudinal sections for principal piece of *Cabyr* KO spermatozoa. A) Medial sections defined by central pair (CP) microtubules (MTs). Rib medial sections exhibit the CP of single MT thickness and two ODFs. LC medial sections passing through doublet MTs 3 and 8 exhibit the CP of two singlet MTs thickness and no ODF. No disruption was observed in LC of *Cabyr* KO spermatozoa (22 fine LCs out of 22 sections examined). B) Lateral-longitudinal sections that do not exhibit CP MT. Ribs ran in a transverse direction in the control (HET). In contrast, ribs running in a vertical direction were observed in the KO. White arrows indicate vertically aligned ribs. C) Analysis of the flagella for vertically aligned ribs. The number of flagellar sections analyzed are indicated above the graph.
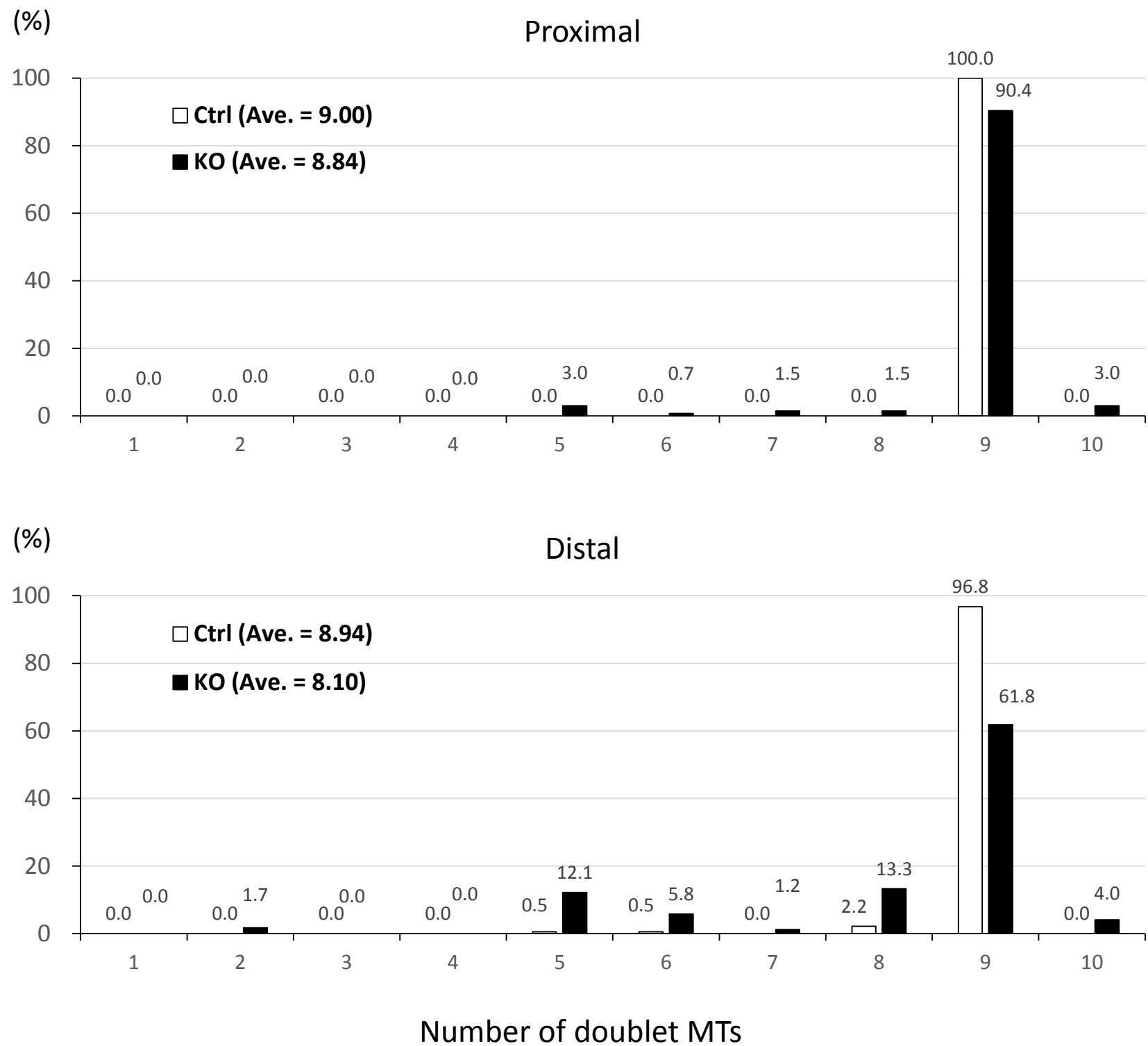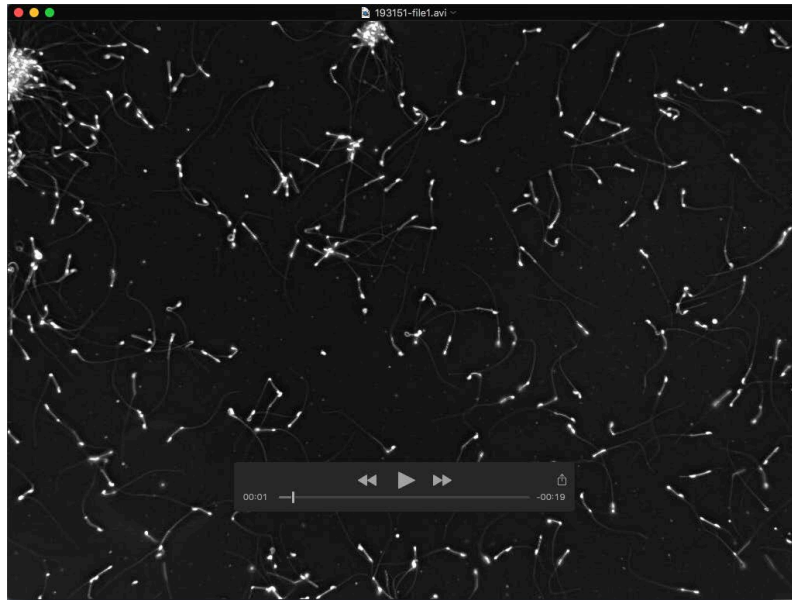
Fig. S4. Ultrastructural analysis of cross sections of the axoneme in the principal piece of *Cabyr* KO spermatozoa. Distribution of the axoneme with different numbers of doublet microtubules in the proximal and distal regions. Abnormal axonemes defined as more or less than 9 doublet microtubules are summarized for Fig. 6E.

Supplementary Movie 1. Spermatozoa of *Cabyr* KO mice at 10 min incubation in TYH media. Movie is shown at 1/5th speed.
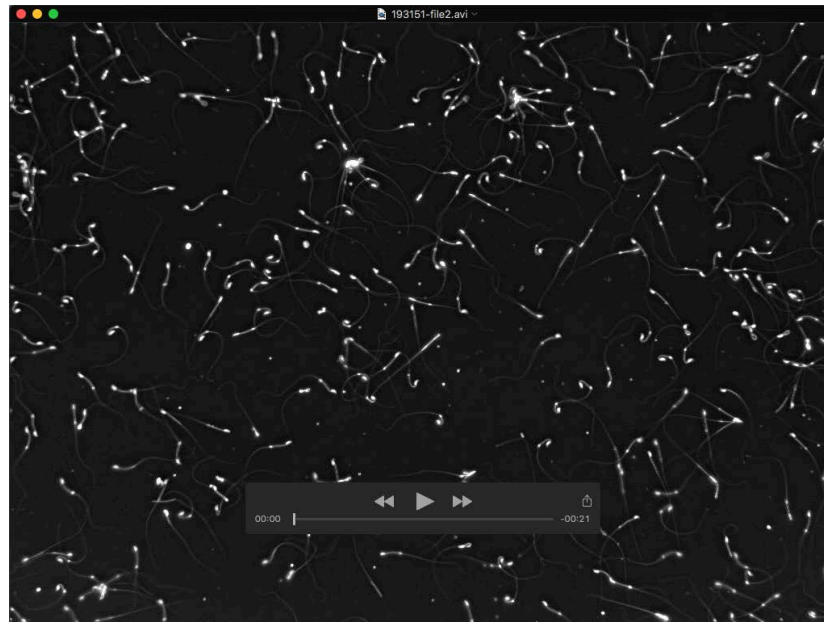
Supplementary Movie 2. Spermatozoa of *Cabyr* HET mice at 10 min incubation in TYH media. Movie is shown at 1/5th speed.